Thesis

Master's degree in material engineering

Finite element analysis of hot rolling in the blooming mill

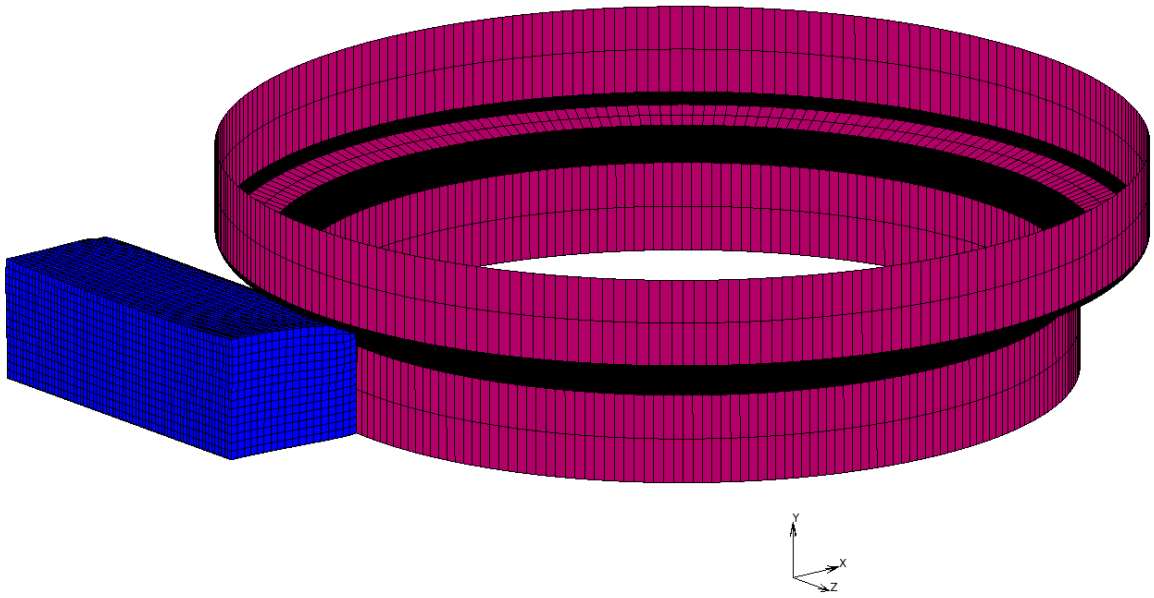

Author: Petter Persson
Mentor at Sandvik: Mattias Gärdsback and Fredrik Sandberg
Supervisor at University of Dalarna: Kumar Babu Surreddi
Examiner: Lars Karlsson
Subject: Materials Engineering
Course: MP4001
Credit: 30 hp
Date of examination: 2016-06-13

Abstract:

During this thesis work a coupled thermo-mechanical finite element model (FEM) was built to simulate hot rolling in the blooming mill at Sandvik Materials Technology (SMT) in Sandviken. The blooming mill is the first in a long line of processes that continuously or ingot cast ingots are subjected to before becoming finished products.

The aim of this thesis work was twofold. The first was to create a parameterized finite element (FE) model of the blooming mill. The commercial FE software package MSC Marc/Mentat was used to create this model and the programing language Python was used to parameterize it. Second, two different pass schedules (A and B) were studied and compared using the model. The two pass series were evaluated with focus on their ability to heal centreline porosity, i.e. to close voids in the centre of the ingot.

This evaluation was made by studying the hydrostatic stress (σ_m), the von Mises stress (σ_{eq}) and the plastic strain (ε_p) in the centre of the ingot. From these parameters the stress triaxiality (T_x) and the hydrostatic integration parameter (G_m) were calculated for each pass in both series using two different transportation times (30 and 150 s) from the furnace. The relation between G_m and an analytical parameter (Δ) was also studied. This parameter is the ratio between the mean height of the ingot and the contact length between the rolls and the ingot, which is useful as a rule of thumb to determine the homogeneity or penetration of strain for a specific pass.

The pass series designed with fewer passes (B), many with greater reduction, was shown to achieve better void closure theoretically. It was also shown that a temperature gradient, which is the result of a longer holding time between the furnace and the blooming mill leads to improved void closure.

Key words: Finite element, FEM, FEA, blooming mill, void closure, hot rolling, pass series

Table of Contents

1 Introduction

During this thesis work a coupled thermo-mechanical finite element model was built to simulate hot rolling in the blooming mill at Sandvik Materials Technology (SMT) in Sandviken. It was made with the commercial finite element (FE) package MSC Marc/Mentat [1] and parameterized with a Python script which simplifies future simulations of different pass schedules. Two different pass series were simulated, each with two different transportation times from the furnace. The different pass series and transport times were evaluated with the focus on their ability to close voids in the centre of the ingot. This evaluation was made by studying the strain penetration in the cross section of the ingot, the hydrostatic stress and the plastic strain in the centre of the ingot.

The strain penetration was studied to gain more knowledge about the inhomogeneity of the deformation in the blooming mill, and the possibility to affect it. Both hydrostatic stress and plastic strain is needed for void closure, which makes them interesting when it comes to evaluation of pass series. These parameters can be calculated using a FE model. To evaluate the mechanical state, the hydrostatic stress was divided by the equivalent stress in the centre of the ingot. This is called stress triaxiality (T_x) and puts the hydrostatic stress in relation to the resistance to deformation of the material. An analytical parameter is also studied, the delta parameter (Δ), which is the ratio between the mean height of the ingot and the contact length between the roll and the ingot $\left(\frac{\bar{h}}{L}\right)$. The parameter Δ is used to investigate if the strain reaches the centre of the ingot and is calculated for each pass.

1.1 Background

The blooming mill (also known as roughing mill) is the first step in a long line of processes that the continuously or ingot cast ingots will be subjected to before becoming finished products. During this process the cross-section of the ingot is diminished step by step through reversible rolling, i.e., the ingot travels forward through the roll gap in one pass and then backwards in the next. The number of passes needed to reach the desired size for the bloom varies, but may be as many as 50. Today there are a lot of different mill setups available. The two-high reversible mill is however widely used and one of the most common for rolling of large products like blooms [2]. This is also the setup that is used in the blooming mill at SMT. The rolls in the blooming mill have both flat and grooved parts which are used at different passes depending on the desired size and shape of the bloom. A schematic representation of a roll of this type is shown in figure 1.

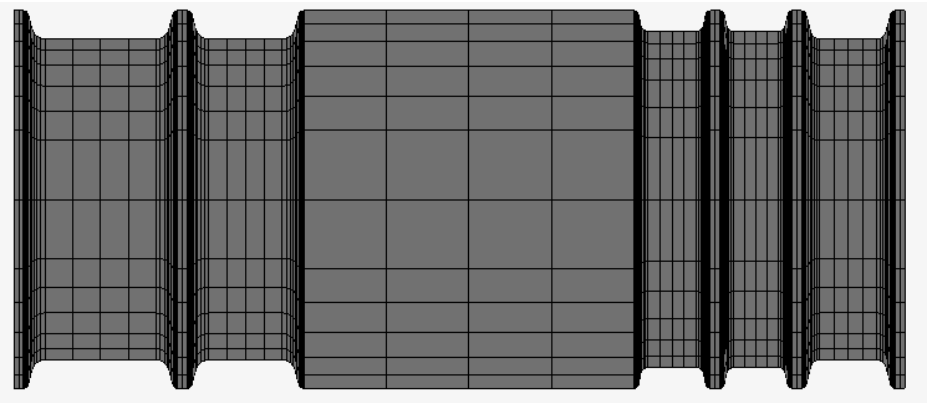

Figure 1. Schematic representation of one of the rolls that is used in the blooming mill.

Before the ingots reach the blooming mill they are reheated in a furnace according to specific time-temperature schedules that differs with steel grade and dimension. Besides lowering the force needed for deformation of the material, the elevated temperature also has other effects. One is that the chemical composition is homogenized due to an increased diffusion rate. Another advantage is that the steel can withstand higher strains without the formation of cracks and other defects. The high temperatures during the deformation of the material also affect the finished microstructure through grain growth and static, dynamic and metadynamic recrystallization.

The combination of many passes and a complex deformation process require simulations that are computationally demanding. However, the continuous improvement in computational capacity has made simulations like this viable, particularly when the simulated process has one or more symmetrical planes. Another difficulty is that every change in the pass reduction scheme or pass series requires a new simulation. To minimize the amount of time required for creating or adapting simulations, the finite element (FE) model was parameterized. This means that a script that use important process parameters as input data was created, which in turn wrote the input file to the FE software.

1.2 Aim

The aim of this thesis work was twofold. The first was to create a FE model of the blooming mill, using the MSC Marc/Mentat software package and parameterize the model using a Python script. This would simplify future simulations of different pass series with the possibility of varying process parameters, e.g. the roll diameter or the material. Secondly, two pass series (A and B) of a 316L austenitic stainless steel grade were studied and compared using the FE model. Pass series A is used in production today and B is a proposed alternative to enhance void closure in the blooming mill. This second part of the thesis was done both to validate the FE model and to gain a better understanding of the blooming mill. Particularly, the effect of varying process parameters in order to eliminate centreline pores was of interest when comparing the two series.

2 Theory

2.1 Material behaviour

The plastic deformation of a crystalline material is due to the movement of dislocations, which are different types of imperfections in the atomic lattice of a metallic material. The atomic planes in the lattice moves in relation to each other, this is called slip. The ease of the dislocation movements is affected both by strain rate and temperature but also by the microstructure of the deformed material. A lower strain rate or higher temperature both lower the stress that is needed for deformation. The microstructure is a product of parameters like strain, strain rate and temperature due to a number of microstructural mechanisms. These mechanisms can both harden and soften the material. In other words, the ability to slip is made harder or easier. During hot deformation, mainly three different mechanisms must be taken into consideration: work hardening, recovery and recrystallization.

Work hardening is an effect of dislocations interacting and hindering the movement of each other. When plastic deformation occurs, the dislocation density increases and during slip some dislocations will meet others and create stress fields. This leads to a greater stress being needed for continued slip.

When dislocations are generated, the distortion of the lattice that they cause leads to an increased state of energy. Both recovery and recrystallization decrease the stored energy in the lattice, i.e., the stored energy is the driving force for these mechanisms. Recovery does this both through dislocation relocation and annihilation. Humphreys and Hatherly [4] describe the recovery process with various stages shown schematically in figure 2. Notable is that these stages may overlap or not occur in the given order (a-e).

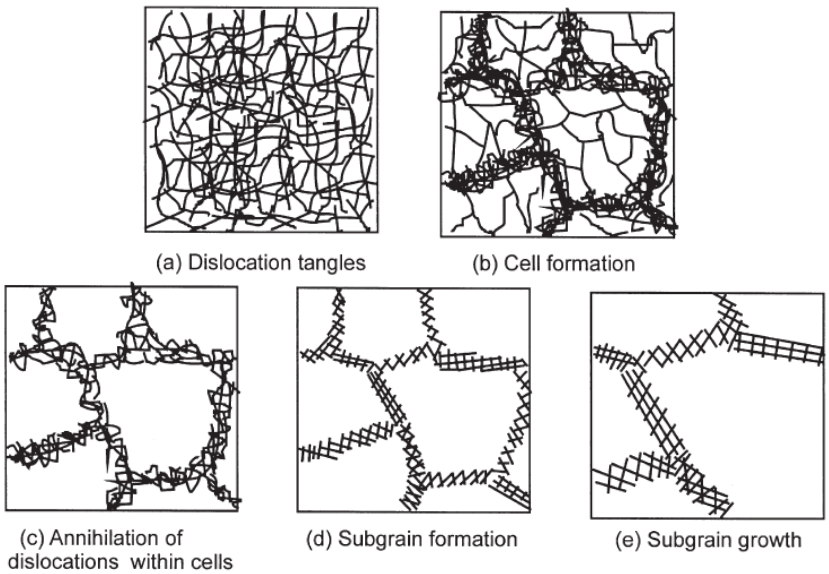

Figure 2. Schematic representation of the different possible steps in the recovery process [4].

During recrystallization on the other hand, the deformed material is replaced with new strain-free grains. This process is divided into two stages, nucleation and growth, both of which can be active at the same time in the material. Humphreys and Hatherly [5] describes the recrystallization nucleus as *"a crystallite of low internal energy growing into deformed or recovered material from which it is separated by a high angle grain boundary"*. After nucleation the strain-free grains grow and replace the deformed grains.

As mentioned above these hardening and softening mechanisms are affected by a number of factors, e.g.: strain, strain rate and temperature. The material behaviour during a forming process is therefore a complex process. Lin and Chen [6] described the mechanisms during hot deformation by dividing a typical true stress-strain curve into four stages, figure 3. In stage 1, the work hardening is greater than the dynamic recovery (DRV) rate and the stress rises. During the second stage, the work hardening competes with both DRV and dynamic recrystallization (DRX), and the stress rises, but at a decreased rate. In stage 3, DRV and DRX annihilate dislocations at a greater speed than the work hardening creates new ones, which leads to a softening of the material. Finally, in stage 4, a balance between hardening and softening is obtained.

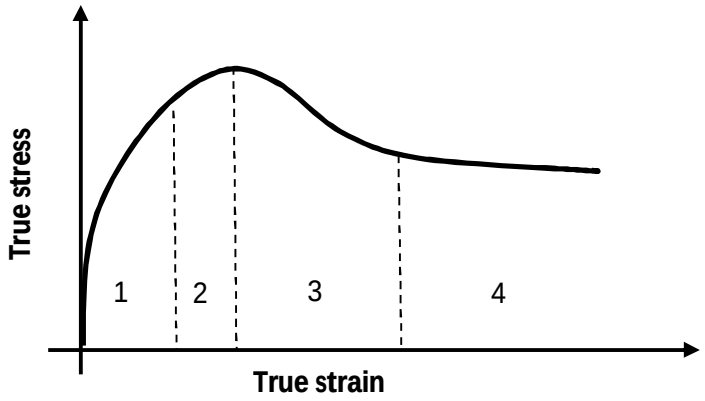

Figure 3. A schematic representation of a true stress-strain curve divided into four different stages during hot deformation where different softening and hardening mechanisms are present as described by Lin and Chen [6].

2.2 Hot workability

When transferring from the laboratory into the industrial process of hot rolling, the complexity increases and the parameters are often kept as industrial secrets [7]. To highlight this difference, the term hot workability is used. The term is used to qualitatively describe the amount of plastic deformation a material can undergo in a specific process without failure occurring. One way of describing hot workability at different temperatures and strain rates is with a processing map (PM), which is shown in figure 4.

In a processing map the efficiency of power dissipation (η) through dynamic metallurgical mechanisms during deformation is plotted for variations of strain rate and temperature. They are based on the principles of the dynamic material model, which views the workpiece as a dissipater of power [8]. The dissipation of power occurs through either an increase in temperature or microstructural change. The power dissipated through dynamical metallurgical mechanisms is called the J content (J). J is defined in equation 1 for a specific temperature and strain, where m is the strain rate sensitivity factor, σ the flow stress and $\dot{\varepsilon}$ the strain rate.

η is the quota of J and the maximum value of J (J_{max}) and indicates how effective the power dissipation through metallurgical mechanisms is. J_{max} occurs when the strain rate sensitivity factor is 1. This leads to η being defined by equation 2. For common engineering material the situation of m being 1 doesn't occur. But the quota of J and J_{max} (η) is an indicator of to what extent mechanism like recovery and recrystallization occur for specific strains with the variation of temperature and strain rate. Even though every process map is produced for a specific strain, it has been shown that the variation in strain does not affect the power dissipation significantly [8]. However, it should be noted that for specific mechanisms like dynamic recrystallization a critical strain is necessary.

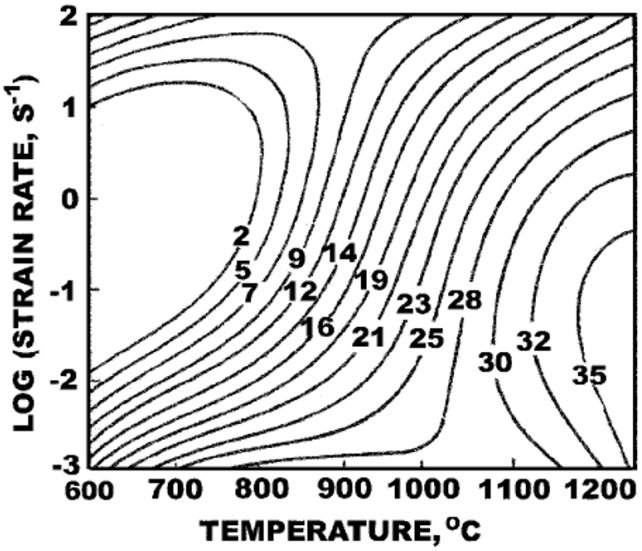

Figure 4. Processing map of the steel grade 316L, showing the efficiency of power dissipation through dynamic metallurgical mechanisms depending on temperature and strain rate [7]**.**

$$J = \frac{m\sigma\dot{\varepsilon}}{m+1} \quad (1)$$

$$\eta = \frac{J}{J_{max}} = \frac{2m}{m+1} \quad (2)$$

The processing map is often combined with an instability map where areas of stable and unstable material flow are defined for different temperatures and strain rates. According to Venugopal and Sivaprasad [7], unstable material flow occurs when the instability parameter $\xi < 0$, where $\xi(\dot{\varepsilon})$ is defined by equation 3. By plotting the variation of this instability parameter with strain rate and temperature an instability map is obtained that shows regions of flow instability.

$$\xi = \frac{\delta ln\left[\frac{m}{m+1}\right]}{\delta ln\dot{\varepsilon}} + m \qquad (3)$$

When combining a processing map and instability map a very useful tool for evaluating different deformation processes is achieved. A number of papers dealing with this approach of combining processing maps and instability maps for austenitic stainless steels have been published [7] [8] [9]. For the specific steel grade 316L the processing map is shown in figure 5 [8]. This shows that for the temperatures of interest in this work (1100-1250 °C) the process in the blooming mill is in a stable region up to strain rates of 10 s^{-1}. It also shows that quite high power dissipation efficiency is achieved at those temperatures. According to the PM in figure 5 the highest power dissipations due to metallurgical mechanisms of 316L, and there for the optimal conditions for dynamic recrystallization are 1250 °C and a strain rate of 0.05 s^{-1}. Strain rates are however not that low in the real process and the rate of dynamic recrystallization decreases as the strain rate increases. According to Venugopal and Sivaprasad [7] dynamic recrystallization does however occur at temperatures over 1110 °C at the strain rate of 1 s^{-1} for 316L.

Important to remember is also the impact of the as-cast structure present in the ingot when it reaches the blooming mill. Mataya et al. [10] showed that this have a big impact on the microstructural evolution. The coarse and columnar structure provides fewer nucleation sites and therefore a smaller volume of the material undergoes DRX if it is initiated at all. The same study looked into the amount of static recrystallization that occurs after compression of as-cast 316L material. They showed that even with a short holding time (2s) the volume fraction of total recrystallized material can be relatively high (38 %) if both the temperature and strain are high (1150 °C and 1 respectively).

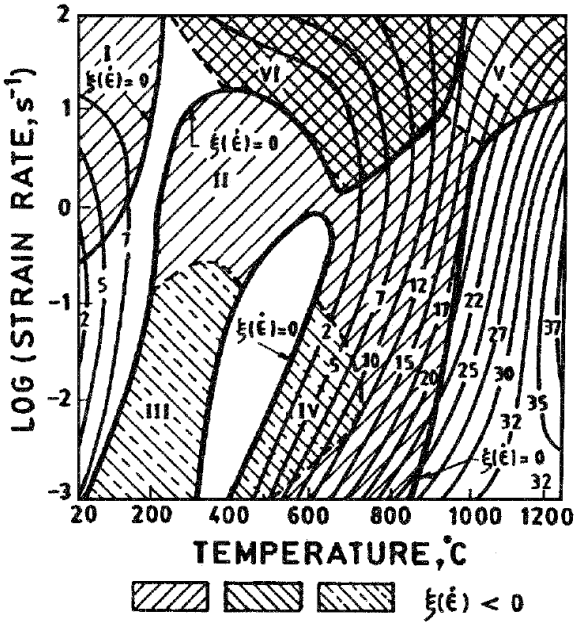

Figure 5. A combined processing map and instability map of the steel grade 316L [8].

2.3 Material models

Calculation of the flow stress is a key part in a FEM-model in order to gain precise results. This is challenging for hot working processes, since the material behaviour is complex, as discussed in chapter 2.2. A variety of constitutive equations, that are either phenomenological or to a varying degree physically based, have been used in simulations of hot deformation of stainless steel [11] [12].

During this work the Johnson-Cook model [13] (shown in equation 4) was used. This equation is not based on the physics of material deformation, instead it is a mathematical fitting of empirical data. The model was proposed 1983 as a way to describe the flow stress for metals and alloys during large strains, strain rates and elevated temperatures.

$$\sigma = [A + B\varepsilon^n][1 + C \ln \dot{\varepsilon}^*][1 - T^{*m}] \quad (4)$$

Where $\dot{\varepsilon}^* = \frac{\dot{\varepsilon}_p}{\dot{\varepsilon}_{p0}}$ and $T^* = \frac{T - T_0}{T_m - T_0}$

The process parameters strain (ε), strain rate $(\dot{\varepsilon})$ and working temperature (T) are used to calculate the flow stress (σ) of the material. A is the yield stress at the reference temperature (T_0) and reference strain rate$(\dot{\varepsilon}_{p0})$. While *B*, *n*, *C* and *m* are called the strain hardening coefficient, strain hardening exponent, strain rate hardening coefficient and the thermal softening exponent respectively. The dimensionless strain rate $(\dot{\varepsilon}^*)$ is the ratio between the strain rate $(\dot{\varepsilon}_p)$ and the reference strain rate $(\dot{\varepsilon}_{p0})$ while the homological temperature (T^*) is a function of the absolute temperature (T), reference temperature (T_0) and melting temperature (T_m) of the material.

2.4 Inhomogeneous deformation

During most rolling processes, deformation takes place in three directions and the stock is subjected to elongation, spread and reduction in the longitudinal, width and vertical directions respectively. During hot rolling in the blooming mill, the strain distribution is inhomogeneous in all three directions.

Near the ends of the ingot, the stress and strain is different due to the special conditions that occur during the start and finish of the rolling process. During the initial contact between the roll and the ingot, the contact length is small and the friction varies between adhesion and slip. After this, the process reaches a steady state until the end of the pass, at which the ingot and roll starts to loose contact, and the contact length once again changes.

In this steady state part of the process, the strain goes from larger in the outer parts of the cross section too smaller in the centre of the stock. According to both Tarnovskii et.al. [14] and Backofen [15], the inhomogeneity of the vertical deformation is the most important character and the cause of other phenomena of inhomogeneity. One important parameter when it comes to the penetration of deformation is the geometry of the deformation zone [14] [15], which is further discussed in the following pages. Another important reason is the occurrence of friction between the rolls and the stock. Other reasons may be the inherent temperature gradient, both in the rolling direction and the cross section of the stock, and differing chemical or microstructural composition of the ingot.

As mentioned earlier, parameters with great impact on the deformation are the geometry of the tools and the geometry of the deformation zone which they affect. The deformation zone can be described by the ratio (Δ) of the mean height of the stock ($\bar{h}$) and the contact length between the tool and the material (L). This ratio has extensively been used to describe the strain gradient in the cross section of a rolled material, e.g. in [14] [15]. During rolling with flat rolls, Δ is calculated according to equation 5 using the simplified expression for the contact length shown in equation 6. The parameters used in this equation are shown schematically in figure 6. A value of $\Delta \approx 1$ describes a process where the strain gradient in the vertical direction is small. As Δ increases or decreases from 1, the inhomogeneity of the strain distribution increases. During rolling in the blooming mill, Δ is larger than 1 and the bigger it gets the more the strain is concentrated close to the surface of the stock. This means that the strain in the centre of the ingot is small when Δ is large.

$$\Delta = \frac{\bar{h}}{L} = \frac{h_{in}+h_{out}}{2*\sqrt{R*(h_{in}-h_{out})}} \quad (5)$$

$$L \approx \sqrt{R*(h_{in}-h_{out})} \quad (6)$$

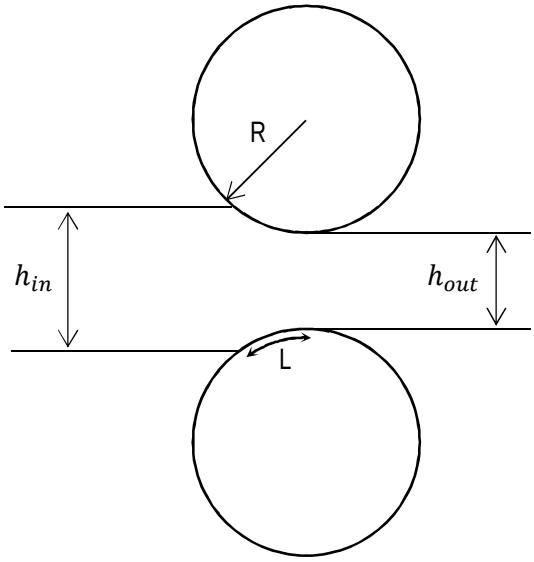

Figure 6. Schematical representation of rolling with the contact length (L), roll radius (R) and ingoing (h_{in}) and outgoing (h_{out}) heights of the ingot.

Dudra and Im [16] compared simulated and experimental data from forging of a square ingot, where plane strain in the square cross-section was assumed in the simulations. Therefore, a deviation between measured and simulated values implies inhomogeneous deformation due to less deformation in the centre. The compressive strain as a function of reduction are shown in figure 7. The simulated values are marked ALPID. The measured data for three different ratios (0.35, 0.45 and 0.55) of contact length and ingot height are shown. Note that the Δ parameter is reversed in this study and the ratio *S/H* is used to indicate contact length/height, (S/H = 0.5 is the same as Δ = 2). The comparison shows that when *S/H* increases, i.e. Δ decreases, the deformation state approaches that of plane strain. For a ratio *S/H* = 0.55 (Δ = 1.82), the deformation is almost homogeneous. This leads to consolidation of material in the centreline. Even though this study was done for forging, similar values of *S/H* should result in good strain penetration, and therefore consolidation of material in the centreline of the ingot for rolling, as well.

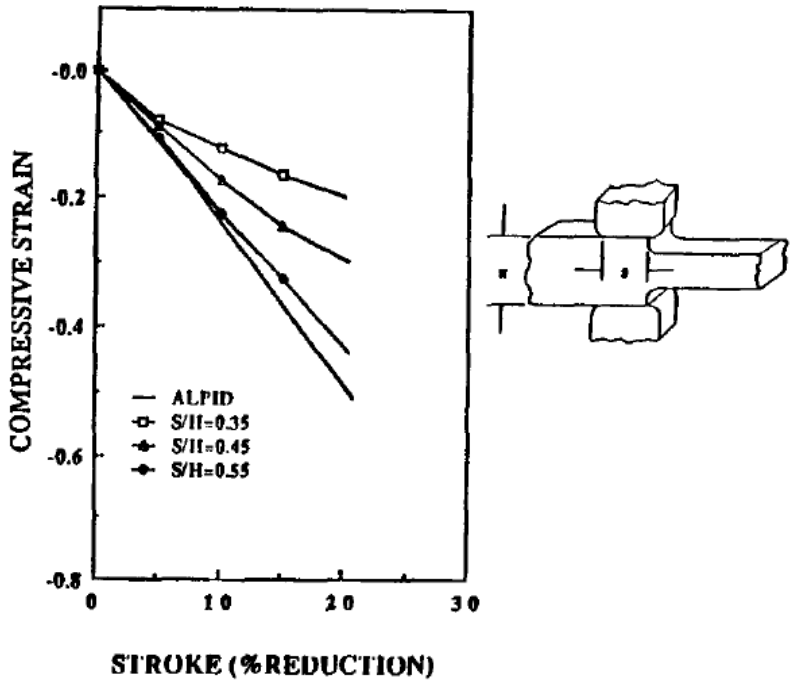

Figure 7. Compressive strain plotted against reduction during forging of a square ingot. Values from plane strain simulations (ALPID) and measured data, using three different ratios of contact length and ingot height (*S/H*), were compared by Dudra and Im [16].

2.5 Void closure

As-cast ingots, which are used in the blooming mill, contain defects to a greater or lesser extent. Types of defects and their extent are dependent on whether they are continuously or ingot cast and of the settings in these processes. One defect is voids in the centre of the stock due to solidification shrinkage or gas entrapment. This defect is common in continuously cast ingots that are most commonly used in the blooming mill. These voids must be eliminated to ensure the mechanical properties of the finished product, and hot working in the form of rolling or forging is used to manage this. The elimination of voids is done in two stages. First the void is closed with mechanical work and then its internal surfaces are bound together. The first stage, i.e. the mechanical closing of voids is examined in this work. Centreline porosity is a defect that isn't usually detected until the quality of the finished product is controlled, causing large costs if products have to be scrapped. This aspect makes the void closure very important during hot rolling of as-cast products, and has led to a lot of work being done and papers published with the focus on elimination of porosity.

In general, the healing of centreline porosity during hot rolling of large cross section ingots can qualitatively be said to improve with the following guidelines: higher reductions during specific passes, increased roll radius and implementation of a temperature gradient in the radial direction of the ingot [17]. Notable here is that both increased reductions per pass and increased roll radius lead to a larger contact length and a smaller value of Δ as discussed in chapter 2.4, equations 5 and 6. Consecutive passes with reductions in the same direction also improve the closure of voids. The groove geometry also influences the material flow and the strain distribution, and thereby the void closure [18]. The influence of changes in the groove geometry would however require an extensive study of effects like roll wear etc. and is not included in this thesis.

2.5.1 Descriptive parameters

Modelling of void closure can be divided into two categories according to Saby et al. [17]. One where the macroscopic scale is studied by varying process parameters and investigating the effect this has on voids with specific shapes and at specific locations in the stock. This category contains studies of both experimental work and finite element simulations. The second category is focused on the micro scale where an analytical prediction of the void volume evolution of an idealized void is made. Both of these categories have drawbacks. The analytical predictions are dependent on theoretical assumptions of the void morphology and the stress and strain state. Using the macro scale approach leads to case dependent models and using the micro scale approach leads to models that don't correspond to industrial cases due to theoretical assumptions [17]. The problem with the macroscopic modelling approach is how to achieve a quantitative measurement of the void closure in a material.

Both types of methods have shown that the combination of plastic strain (ε_p) and hydrostatic stress (σ_m) is of importance for void closure. The hydrostatic stress is the mean value of the principal stresses, as shown in equation 7. With compressive stresses dominating, this value becomes negative, i.e. there exists a hydrostatic pressure. To further describe the mechanical state, the hydrostatic stress is divided by the von Mises stress. This ratio is called the stress triaxiality (T_x) and relates the hydrostatic stress to the deformation resistance of the material (equation 8). Saby et al. [17] compared a number of models predicting void closure for different values of T_x. The plastic strain needed to close voids was shown to vary for different T_x, and for different types of material. However, the most stable models predicted a remaining void volume of ~20 % compared to the initial, when reaching plastic strains over 0.4.

$$\sigma_m = \frac{\sigma_{11}+\sigma_{22}+\sigma_{33}}{3} \tag{7}$$

$$T_x = \frac{\sigma_m}{\sigma_{eq}} \tag{8}$$

One parameter that has been used as an indication of void closure and includes both plastic strain and stress triaxiality is the hydrostatic integration parameter (G_m) that is calculated according to equation 9.

$$G_m = \int_0^{\varepsilon_f} \left(\frac{-\sigma_m}{\sigma_{eq}}\right) d\varepsilon \tag{9}$$

2.5.2 Void shape

The morphology (size and shape) of a void and its location in the studied material are of great importance when it comes to closing it. Saby et al. [19] highlight this with FE simulations of ellipsoidal voids that were based on observations of voids from the industry. They could show that the model using ellipsoidal voids had a smaller prediction error than others that used spherical voids.

In the review article [17] a number of different models where compared. It showed that models that used FEM as a base, and therefore took into account the change in void shape during deformation, were less dependent on a large hydrostatic pressure. These models showed a dependence on the hydrostatic pressure only in the first stages of deformation. After the spherical shape of the void had been weakened, the plastic deformation played a bigger role than the hydrostatic pressure. Since real voids do not have a perfectly spherical shape, plastic deformation can be assumed to have a greater impact on void closure than hydrostatic pressure. This is not taken into account in the G_m parameter which makes it less suited to predict results in industrial applications. Despite this, G_m is still useful as a comparative parameter and if there is a need to use a single scalar in the evaluation of void closure.

2.5.3 Change of load direction

A problem for evaluation of the void closure ability is the fact that the ingot is turned between some of the passes in the blooming mill. The effect of a change of load direction was shown by Saby et al. [20] by using simulations with representative volume elements (RVE) where the load direction was alternated between the z- and x-axis according to table 1. The simulations where performed with different void shapes. Results for two of the shapes are shown in figure 8. Figure 8 a) shows the results using a void morphology which was determined using x-ray examination of real steel ingots and 8 b) the results using a sphere to describe the void. When the direction of loading is changed from one axis to another (turned by 90 °), the total plastic deformation required to close the void increases. This effect is most prominent when the simulated void has the shape of a sphere, even though the same trend is visible in simulations using a realistic void morphology. The main reason is that it is easier to close a void by compressing it along its smallest direction. For a sphere, the void has the same length in all directions, while a real void is more elliptical and its length is smaller in both directions X and Z.

Table 1. Compression axes for all tested cases for non-uniform loadings [20].

Interval	[0-1 s]	[1-2 s]	[2-3 s]	[3-5 s]	[5-10 s]
Case A	Z	Z	Z	Z	Z
Case B	Z	X	X	X	X
Case C	Z	X	Z	Z	Z
Case D	Z	Z	X	X	X
Case E	Z	Z	Z	X	X
Case F	Z	Z	Z	Z	X

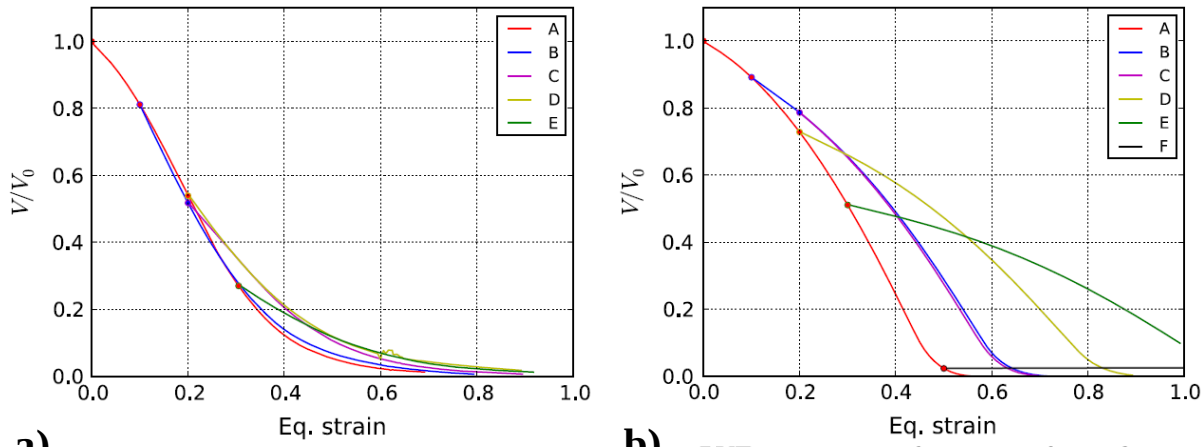

Figure 8. The plastic deformation needed to close a void and the effect of a change of load direction as shown in table 2 according to Saby et al. [20]. Figure a) shows the results using a realistic void morphology and b) the results when using a spherical void.

3 Finite element model

The finite element method (FEM) is a numerical method of solving field problems that are described by differential equations or integral expressions [21]. It is used in a number of fields such as solid mechanics, heat transfer and many more. FEM provides an approximate solution of a problem by dividing a structure into a number of small elements, in which the quantity of interest is only allowed to have a simplified spatial variation [21].

The blooming mill process was simulated using the commercial FEM package MSC Marc/Mentat [1]. In this package the pre- and post-processing is done in the software Mentat. Using this program, an input file is created and sent to the solver Marc. Using Mentat, a model containing the geometry of the active roll grooves for each pass and a meshed representation of the ingot was constructed. For every pass a load case was set up where the time for every pass and the time for the ingot to be reversed and ready for the next was estimated. The time stepping scheme multi-criteria was used with a minimum fraction of the load case time as the lower limit for each time step. This minimum fraction was set so that the smallest allowed step was approximately 10^{-4} seconds (ranging from $9.75*10^{-5}$ to 10^{-4}).

3.1 Assumptions and boundary conditions

The thermo-mechanical situation that occurs during hot rolling means that the FEM-model will be computationally heavy. To lower the calculation time, one quarter of symmetry was assumed for the ingot and rolls, and the length of the ingot was reduced. The assumption of quarter symmetry resulted in an idealized process. However, quarter symmetry of this type has been utilized successfully with the FEM package MSC Marc/Mentat in a number of papers [22] [23] dealing with the simulation of rolling. Yuan et al. [22] simulate continuous multi pass rolling, of type 304 stainless steel, with quarter symmetry and a shortened length of the billet, and showed that the simulated surface temperature agreed well with measured values. In ref. [23], simulations of continuous multi-pass rolling and prediction of the final grain size was done for a high carbon bearing steel with good agreement to measured ones. The symmetry of the cross section of the ingot was maintained with the help of boundary conditions which fixed the nodes in the two symmetry planes in the x- and y-direction respectively. Despite the successful use of this assumption in different papers it should be pointed out that for example no bending of the bloom was allowed in the model which is known to happen in the blooming mill. When shortening the ingot to reduce computing time, care is taken that a steady state section is attained between the starting and finishing part of the bloom. The final length of the ingot was set to 0.35 m in the model.

Another boundary condition in the symmetry planes was that the heat flux was zero. This follows due to the assumption that the thermo-physical properties of the material and the temperature of the ingot are homogeneous when it comes out of the furnace. This is not strictly true, in reality there is a temperature gradient in the cross section of the ingot even as the ingot leaves the furnace. Furthermore, the beams that the ingot rests on in the furnace can contribute to “cold spots” in its longitudinal direction. The initial temperature of the ingot was set to 1250 °C and two different transportation times (30 and 150 s) from the furnace to the blooming mill were used. During the entire simulation the room temperature (T_R) was assumed to be 25 °C.

Boundary conditions were also used to define the heat flux from the ingot to the surrounding environment. This was done by defining the emissivity of the ingot as 0.8 and the natural convection coefficient as 10 W/m^2K for the outer surfaces of the ingot.

Another assumption was that the material that had been deformed in a pass reached full recrystallization before the next pass. This is a simplification that isn't in fact true but together with other softening mechanism such as recovery, the presence of recrystallization does lead to reduction in stresses before the next pass. To simulate this effect an additional annealing load case, which resets the stress and strain state in the material, was used between every pass.

3.2 Geometry

As mentioned earlier the process was viewed as being one quarter symmetric. This meant that the cross section of the meshed ingot could be reduced to one quarter of its real size. It also affected the rolls; only half of the grooves for one roll had to be defined. During this work a roll diameter of 1000 mm was used and the geometries of the different grooves were copied from blueprints. In figure 9, the geometries of the ingot and the roll groove from pass number 3 in series A are presented. While the ingot is meshed and defined as deformable, the rolls are defined as rigid surfaces. For each pass the specific roll groove was modelled and positioned according to the intended roll gap. Some rolls were also rotated 90°, this was done to simulate turning of the ingot, which is done between some of the passes. This lead to a somewhat chaotic looking geometry since the grooves cross each other's paths. However, the surfaces are defined to not interact with each other at all and only at specific times with the meshed ingot.

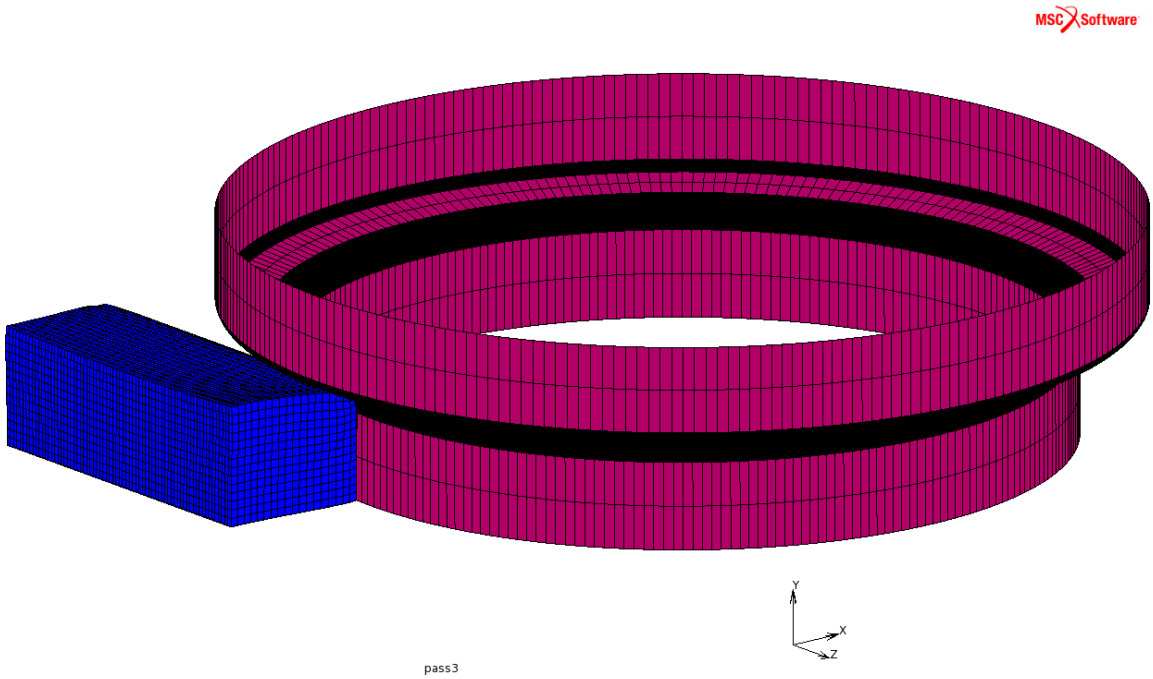

Figure 9. The geometry of a modelled roll groove and ingot after a pass in series A. This represents a quarter of the ingot and half of one of the roll grooves that can be seen in figure 1.

3.3 Contact

The contact between roll and ingot was an important part of the simulation since it is a big contributor to the complexity of it. Two different types of boundary descriptions were used; for the surfaces defining the rolls it was analytical and for the meshed ingot it was discrete. The numerical procedure "node to segment" was used and a contact table that defined when a specific roll was in contact with the ingot was created for every pass.

For contact between rolls and ingot, two different interactions were defined: friction and heat flux. Coulomb friction was used with a bilinear numerical implementation that is based on the relative displacement between the contact bodies. When the relative displacement between two bodies is smaller than a given value (slip threshold) sticking is simulated [24]. The constant friction coefficient μ=0.5 was used in the model, which is a simplified way of describing friction.

Heat flux between ingot and rolls is described by equation 10 [24], where T_1 is the surface temperature of the roll, T_2 is the temperature of the ingot that is in contact with the roll and H_{TC} is the heat transfer coefficient. In the model a heat transfer coefficient of 5000 W/m^{2}K was used and the rolls were assumed to have a surface temperature of 200 °C.

$$q = H_{TC}(T_2 - T_1) \tag{10}$$

3.4 Johnson-Cook material parameters

Data from a number of compression tests of 316L that had been carried out in previous work [25] in collaboration with Sandvik, was used to determine the Johnson-Cook parameters. The compression tests were performed in a Gleeble thermo-mechanical simulator with various constant temperatures and strain rates. In this work, test curves at 1100 and 1300 ° C with strain rates of 1 and 10 s^{-1} were used. Both temperature and strain rate intervals were selected to represent the parameters in the process. For each combination of temperature and strain rate two data series were used.

First, approximate values for the Johnson-Cook parameters (see equation 4) were attained by curve fitting of each data series separately using Matlab. This was done with the least square method, using the interval [0,1] for parameters *n*, *C* and *m*. Parameters *A* and *B* were restricted to positive values, $\dot{\varepsilon}_{p0} = 0{,}1$, $T_0 = 25\,°C$ and $T_m = 1420\,°C$ were used. The obtained values were then used as starting points to describe the material flow for the entire temperature and strain rate interval. To do this, the data from each compression test was plotted. In the same plot, a curve representing the Johnson-Cook equation was implemented for each temperature and strain rate that had been tested, and the parameters where adjusted to reach as good a representation as possible. Noticeable is that the melting temperature had to be increased in the model to achieve good representation in this specific interval of temperature and strain rate.

At this point the material model was tested by running a simulation of pass series A for which logged values of roll separating force were obtained. This showed that the used Johnson-Cook parameters resulted in a roll force that was almost twice as high as the measured. That the material model would have to be tuned to represent the hot rolling process was expected but not that the difference would be that big. One possible reason for this big difference is that the 316L steel that is rolled in the blooming mill have an as-cast structure while the 316L that had been used in compression tests, had gone through a long line of manufacturing processes which affect the mechanical properties. It is also important to remember that the stress state is

not the same in compression tests and rolling. Even though the simulated and measured roll force differed greatly, they followed the same trend. Therefore, the Johnson-Cook parameters A and B were adjusted to lower σ_m uniformly. The resulting difference between the compression tests and the Johnson-Cook equation with the final parameters are shown in figure 10. The final parameters used in the model are shown in table 2. Without the possibility of calibrating the material model against measured separating roll force, it would not have been able to represent hot rolling in the blooming mill.

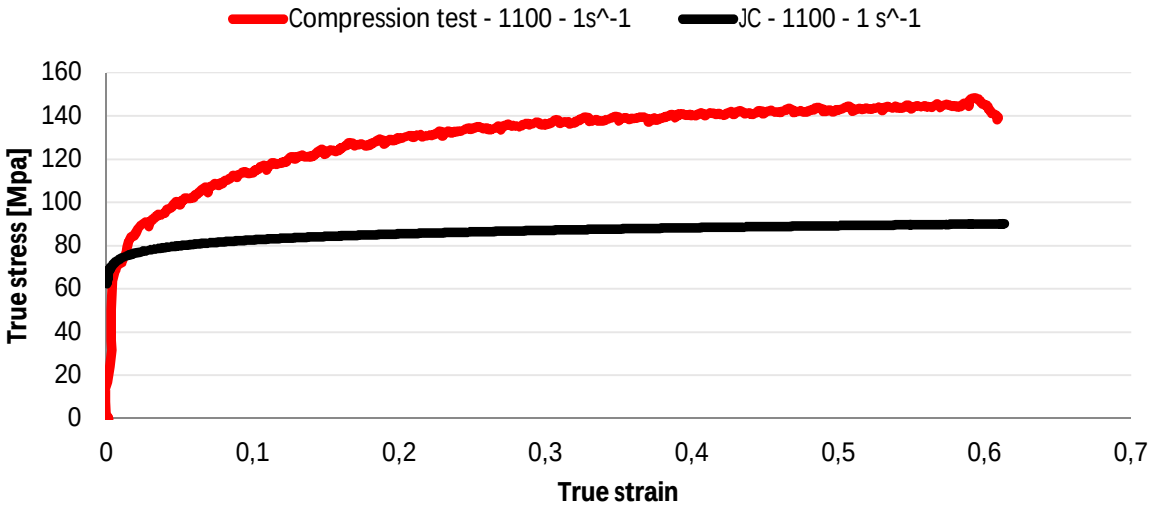

Figure 10. Comparison of a compression test and the final Johnson-Cook parameters for the steel grade 316L at 1100 °C and $\dot{\varepsilon}_p$=1.

Table 2. The parameters that were used in the Johnson-Cook model.

A [Pa]	B [Pa]	n	C	m	T_0 [°C]	T_m [°C]	$\dot{\varepsilon}_{p0}$[s^{-1}]
24*10^6	540*10^6	0.15	0.55	0.325	25	1540	0.1

3.5 Thermo-physical properties

In addition to the flow behaviour of the material, the parameters density (ρ), Young's modulus (E), Poisson's number (ν), heat capacity (C_p) and conductivity (λ) had to be defined in the model. The values of the first three parameters are shown in table 3. Heat capacity and conductivity were defined as functions of temperature according to equations 11 and 12, respectively, and tables were used to define them in Marc/Mentat. All values are based on the works by M. Fukuhara et.al [26] and K. C. Mills et.al. [27]. They should be treated as approximate values, in particular the parameters that are set as constants, which in reality vary with temperature.

Table 3. Values of the parameters density, Young's modulus and Poisson's number.

Density (ρ)	Young's modulus (E)	Poisson's number (ν)
7400 [kg/m^3]	180 [GPa]	0.38

$$C_p = 472 + 0.136 * T - \frac{2.82*10^6}{T^2} \quad \text{[J/kgK]} \qquad (11)$$

$$\lambda = 14.158 + 0.0134 * T \quad \text{[W/mK]} \qquad (12)$$

3.6 Parameterization

When a working FEM-model of the process had been achieved, this was used as a template for making a parameterized script that could recreate the model for different pass series. A procedure file that documented the commands that was used in Mentat to create the working simulation was made. This procedure file is basically a way of recording the commands that is used during the building of a model. It can then be used to "play back" these commands and create a simulation. The use of these procedure files are however limited since no logical operators (if, and, or) can be incorporated.

This problem was solved by using the programming language Python. Using Python and incorporating logical operators and variables, made it possible to efficiently parameterize the model. Python was used due to its incorporation in Marc/Mentat with the modules PyMentat and PyPost. These modules allow for functions that are specific for Marc/Mentat to be used. With the script *"py_create.py"* [28], that is shown in appendix A, the commands in the procedure file was wrapped in the function py_send. A Python (.py) file with these commands was created. This file was used as a starting point and modified by incorporating variables, lists and operators that enabled it to be used for different pass series. The input required for this file is shown in table 4 where variables and lists are presented with a short comment.

Table 4. The required variables and lists for the final parameterized python script with short comments and their units.

Variable	Comment
N	Number of passes
D	Roll diameter [m]
W	Ingot width [m]
H	Ingot height [m]
xs	Number of elements in the x-direction
ys	Number of elements in the y-direction
zs	Number of elements in the z-direction
zl	Length of the elements in the z-direction
my	Friction coefficient in the interface roll / ingot
K	Heat transfer coefficient in the interface roll / ingot [W/m^2K]
T_i	Initial temperature of the ingot emerging from the furnace [° C]
t_f	Holding time between the reheating furnace and blooming mill [s]
t_p	Time allocated for each pass [s]
List	Comment
passID	Specification of which roll groove that is used (1-6) for every pass.
halfRollGap	Measurement of the roll gap / 2 for every pass. [m]
turned	Rotated (90°) position of ingot in relation to the first pass where 0 = not rotated and 1 = rotated.
vIn	Roll velocity [m/s]

3.7 Validation of the FEM model

To validate the model, measured and simulated values of roll separating force and surface temperature of the ingot were compared for pass series A with a 30 seconds transportation time which is in production today. The peak values of the measured roll separating force for 6 ingots are shown together with simulated ones in figure 11. For the same ingots, the surface temperatures were also measured. This was done in the middle of the upper side of the ingot, before every uneven pass, using an infrared pyrometer. The measured surface temperatures are compared with simulated values in figure 12. Both force and temperature are normalized in figure 11 and 12 by dividing each measured or simulated value with the highest measured one. Roll force and surface temperature were measured on the same 6 ingots and should therefore display the coupled thermo-mechanical effect that for example deformation heat has on the process.

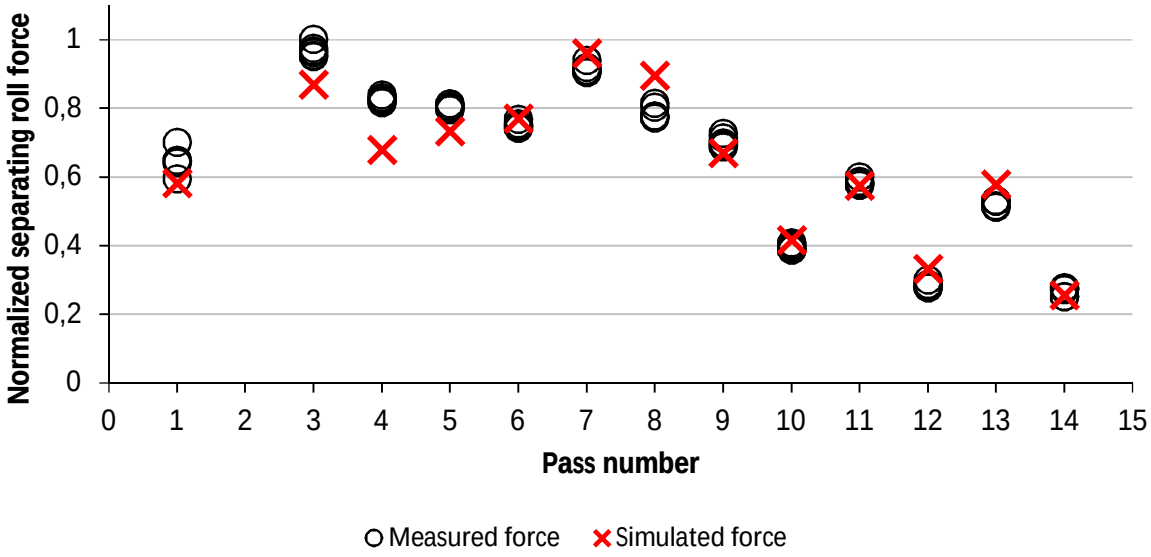

Figure 11. Measured (6 values) and simulated maximum roll force, for each pass during pass series A, using a transporting time of 30 seconds.

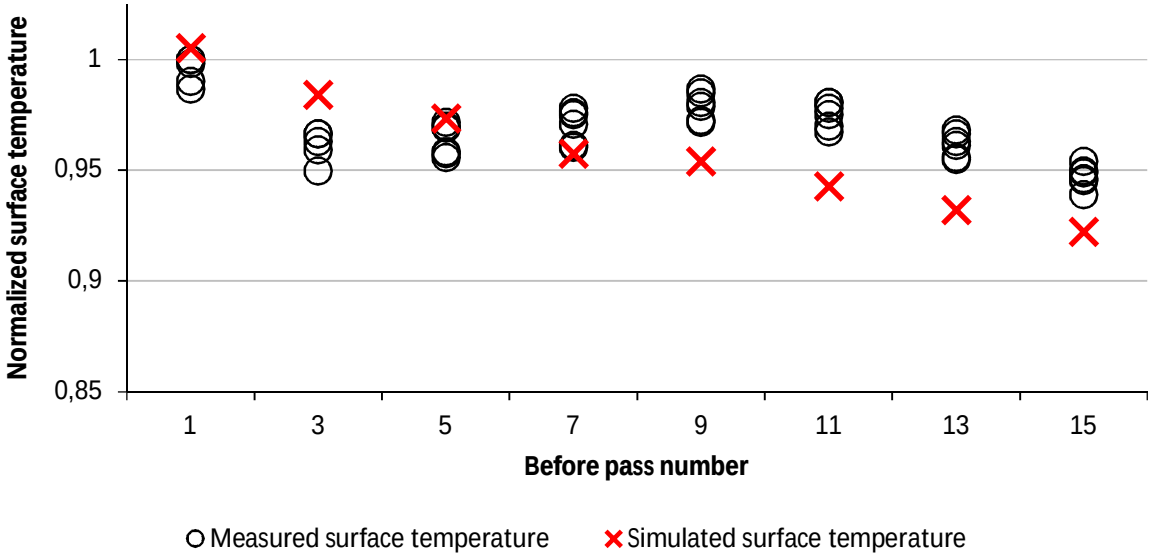

Figure 12. Measured (6 values) and simulated ingot surface temperatures, before every uneven pass during pass series A, using a transporting time of 30 seconds.

Both measured roll force and surface temperature have some built in uncertainties. The measured roll force should be reliable since the same load cells that measured it are used to control the process, and are calibrated. For the temperature measurements, greater variations are anticipated. These were done using a handheld pyrometer in the industrial environment of the blooming mill. This can lead to variations in the location of the measurement on the ingot and the distance between the ingot and the pyrometer. Despite this, the variation of the measured values is small, both for the separating roll force and the surface temperature. The fit between simulated and measured values is quite good when roll force is considered, both when it comes to actual values and the trend of the values. The surface temperature of the ingot does not show the same fit when it comes to the trend. This is especially true for passes 4-9 where the measured temperature rises due to friction- and deformation heat. The simulated values for these passes does instead keep on dropping, with the only change in the trend between passes 7-9 where the drop is smaller than for the others. Despite the trend of the temperature change not fitting, the difference in actual values is not big. It is important to note, however, that this is after tuning the parameters in both the material and thermal model. Since the simulated roll forces and surface temperatures corresponds well with measured values, the model is assumed to represent hot rolling in the blooming mill fairly well.

4 Trial plan

4.1 Material

In both pass series the steel grade 316L was used. The 316L grade is an austenitic stainless steel with the composition shown in table 5 according to the UNS S31603 standard [3]. It has a FCC structure and, due to its low stacking fault energy, twinning easily occurs. The low carbon content ensures good resistance against intercrystalline corrosion and in this specific steel grade some molybdenum is added. This is done to increase the resistance against corrosion in acid environments and in the presence of chloride ions. Since molybdenum is a ferrite stabilizing element, it is necessary to increase the content of nickel compared to grades without molybdenum to ensure that the austenitic phase is stable.

Table 5. Composition of the steel grade 316L according to the UNS S31603 standard [%].

C	Si	Mn	P	S	Cr	Ni	Mo	N
0 - 0.03	0 - 0.75	0 - 2	0 - 0.045	0 - 0.03	16 - 18	10 - 14	2 - 3	0 - 0.1

Due to the good resistance against corrosion in environments with low pH and chloride ions, the 316L grade is commonly used in marine environments, heat exchangers, pipe lines, cooling and heating coils.

4.2 Pass series

During this thesis two different pass series were simulated and analysed, pass series A and B, which are shown in table 6. Pass series A was used to validate the FE model through measured roll forces and surface temperatures from the blooming mill at Sandviks plant in Sandviken. Series B is a modified version of A that is designed to achieve better void closure in the centre of the ingot by improving key parameters discussed in chapter 2.4. The main difference in the pass series is that B have fewer active passes but higher reductions compared to A. Both series are simulated at two different transporting times from the furnace (30 and 150 seconds to evaluate the effect of a distinct temperature gradient in the cross section of the ingot.

Table 6. Comparison of the pass series A and B with regards of area reduction per pass, total area reduction after each pass and when the ingot is turned.

Pass series A			Pass series B		
Pass number	Area reduction per pass [%]	Total area reduction [%]	Pass number	Area reduction per pass [%]	Total area reduction [%]
1	3.36	3.36	1	3.36	3.36
2	0	3.36	2	0	3.36
Turned 90°			Turned 90°		
3	8.08	11.17	3	8.99	12.06
4	6.33	16.79	4	9.66	20.55
5	6.82	22.47	Turned 90°		
6	7.45	28.25	5	4.73	24.30
Turned 90°			6	0	24.30
7	12.13	36.95	Turned 90°		
8	10.86	43.80	7	13.74	34.70
Turned 90°			8	12.38	42.79
9	8.77	48.73	Turned 90°		
Turned 90°			9	10.73	48.93
10	2.92	50.23	10	11.14	54.61
Turned 90°			Turned 90°		
11	6.94	53.68	11	8.63	58.53
Turned 90°			Turned 90°		
12	1.73	54.48	12	1.79	59.27
Turned 90°			Turned 90°		
13	7.07	57.70	13	0	59.27
Turned 90°					
14	0.9	58.08			
Turned 90°					
15	0	58.08			

5 Results and discussion

The FE model was used to gain information about hot rolling in the blooming mill by evaluating the stress-strain state both during and after the two pass series. This could be done after validation of both the thermal and structural parts of the model, which was discussed in greater detail in section 3.7.

The parameterization of the model through the programing language Python served two purposes. Firstly, it saves time for future simulations of different pass series, which was the intended result from the beginning of the thesis. A second beneficial result of the parameterization is that modifications of the settings are easily performed, traceable and only performed if an active choice is made in the Python script. This is of great importance in a simulation with lots of different load cases, different boundary conditions etc.

5.1 Deformation behaviour in relation to the parameter Δ

In figure 13, the plastic strain rate during pass 4 and 7 in pass series B, with Δ values of 2.34 and 1.74 respectively, are shown. From the figure, it is evident that the strain rate increases markedly in the centre of the ingot, at the same time as the strain rate at the surface only increases slightly, when Δ gets closer to 1. This confirms that the strain gradient decreases, and that the deformation reaches the centre when Δ approaches 1. Since the delta parameter is purely geometrical, no comparison was performed for different transportation times. It should also be mentioned that these passes were selected due to the difference in Δ values and that the same roll groove was used.

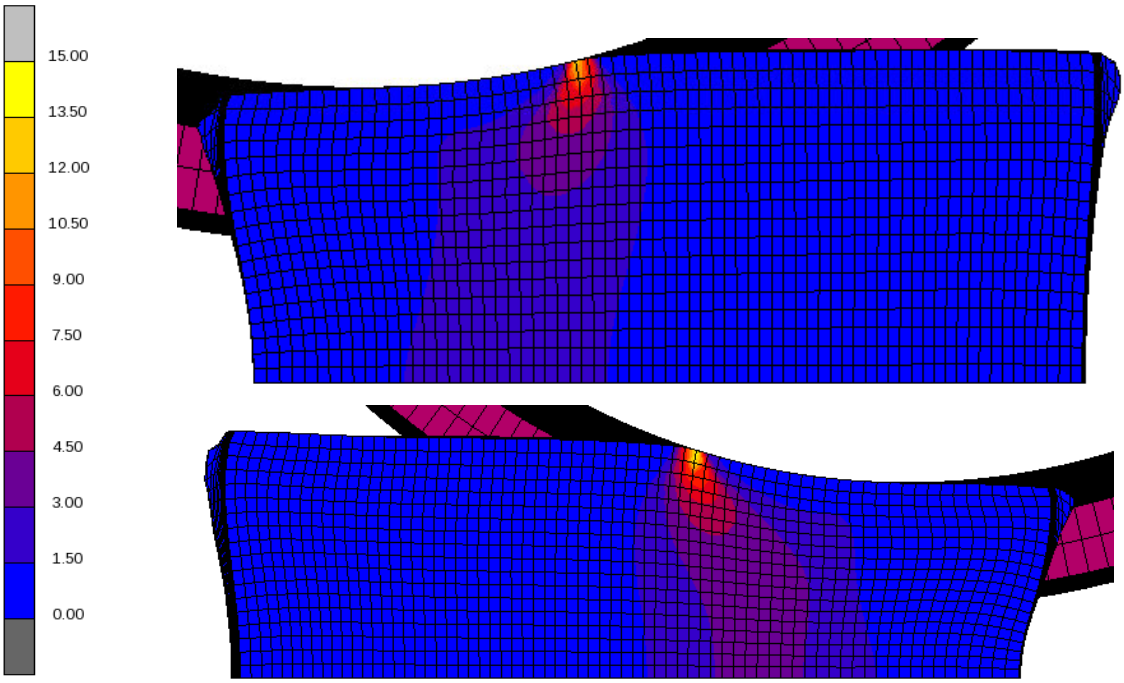

Figure 13. Strain rate $(\dot{\varepsilon})$ for pass 4 (a) and 7 (b) in series B (30 seconds transportation time), with Δ values of 2.34 and 1.74 respectively.

5.2 Distribution of plastic strain

The variation of total plastic strain in the longitudinal symmetry plane, after all passes, for pass series B, with 30 seconds transportation time from the furnace, is shown in figure 14. Even though the values differ in the other simulations, the trend in figure 14 is representative for all of them.

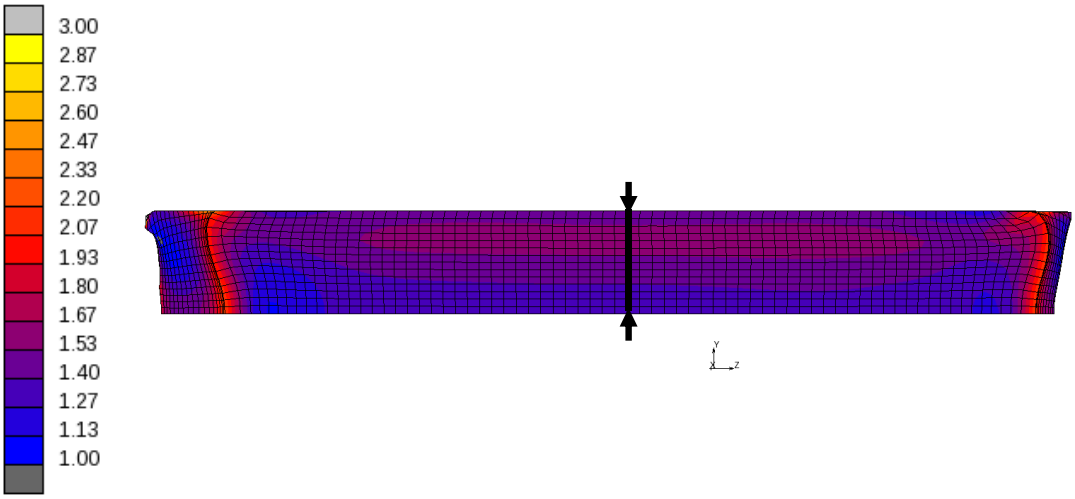

Figure 14. The equivalent plastic strain (ε_p) in the longitudinal symmetry plane of the ingot after series B, using 30 seconds as transport time from the furnace. The cross section that was used to evaluate the different simulations is marked in the centre of the ingot lengthwise.

Because of the special conditions in the first and last parts of the ingot in each pass, when the contact between the rolls and the ingot is initiated and released, respectively, the deformation is inhomogeneous in the longitudinal direction of the ingot. To obtain results that can represent the main part of the process, it is important that the simulations reach a steady state in the middle part of the ingot, which can be seen in figure 14. Because of this, the cross sections that were used to evaluate the pass series were taken from the middle of the ingot lengthwise.

In figure 15, the total plastic strains, in a cross section of the bloom, are shown for simulations of both pass series and using both 30 and 150 seconds transportation time from the furnace to the blooming mill.

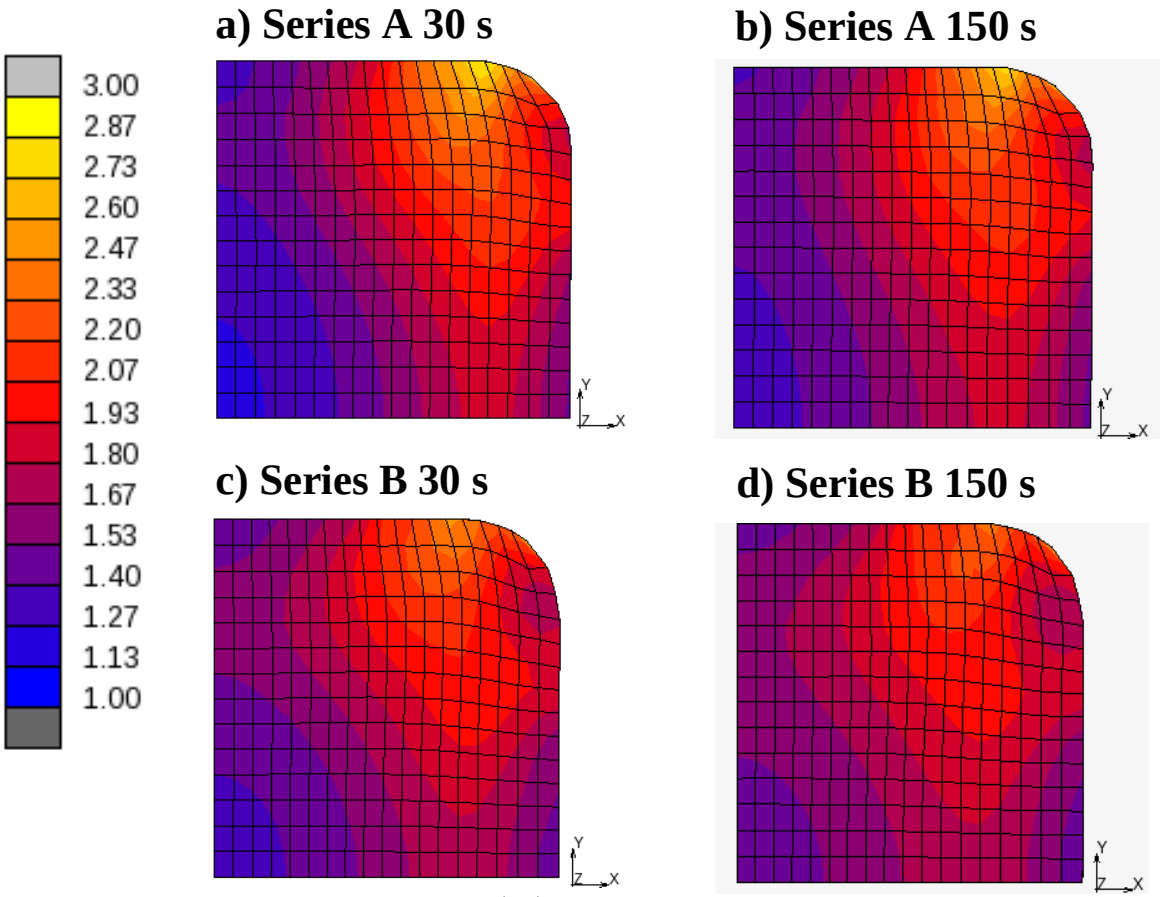

Figure 15. The equivalent plastic strain (ε_p) in the cross section of the ingot after simulation of (a) series A using 30 seconds transportation time, (b) series A using 150 seconds transportation time, (c) series B using 30 seconds transportation time and (d) series B using 150 seconds transportation time.

The cross sections in figures 15a and c show that the strain penetration improves in pass series B in comparison with A. The same is true when comparing 15b and d. Note that the area of interest is the lower left corner of each figure, i.e. the centre of the full sized ingot which is represented by quarter symmetry in the simulations. This is in agreement with theory that says that fewer passes, with larger reduction rates, lead to improved strain penetration. By comparing the distribution of plastic strain in figures 15a-b and 15c-d, respectively, it is also evident that an increased temperature gradient, which is a result of increased transport time from the furnace, leads to increased strain penetration.

An increased temperature gradient is however hard to utilize in practice. The introduction of 120 seconds down time with the ingot in full contact with air is not practical in reality. The reasons are: partially, because it disturbs processes down the line in the process chain, and partially, because of problems to achieve reproducibility of the rolling temperature and other process parameters.

5.3 Stress triaxiality vs. Plastic strain

In figure 16 the stress triaxiality in the centre of the ingot is plotted against plastic strain for pass series A, using a 30 second transportation time from the furnace. It shows that series B contains more passes with both high stress triaxiality and high plastic strain in the centre of the ingot compared to A. Especially interesting are passes 7 and 8, since the load direction is the same and the stress triaxiality is almost the same for these passes in both series. For series A, these two passes achieve a total plastic strain of 0.387, and for series B, this value increases to 0.440. As discussed in section 2.6.3, high plastic strain before change of load direction is desirable to achieve better void closure.

It should also be pointed out that passes 9 and 10 in series B have the same load direction, while the bloom is turned between each pass in series A after the eighth pass. It is difficult to assess the effect of this without extensive industrial tests.

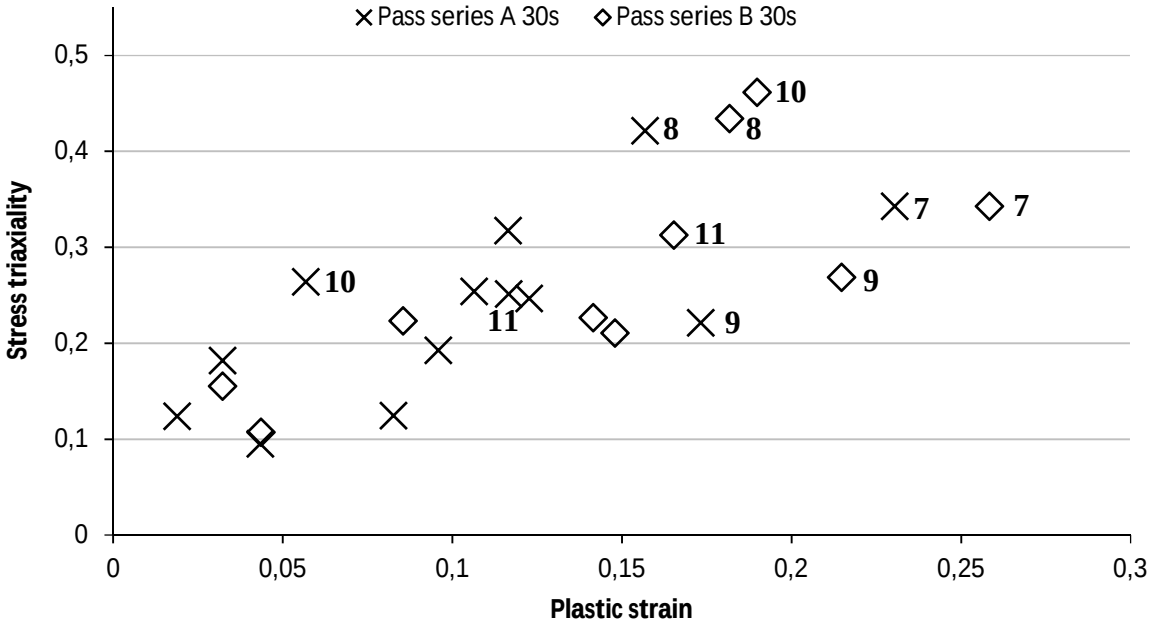

Figure 16. Stress triaxiality $\left(-\sigma_m/\sigma_{eq}\right)$ plotted against plastic strain in the centre of the ingot for all passes in series A and B with 30 seconds transportation time from the furnace.

The result of increasing the transportation time from the furnace for series A is shown in figure 17. The resulting temperature gradient leads to an increase in stress triaxiality and/or plastic strain, which in turn leads to better void closure.

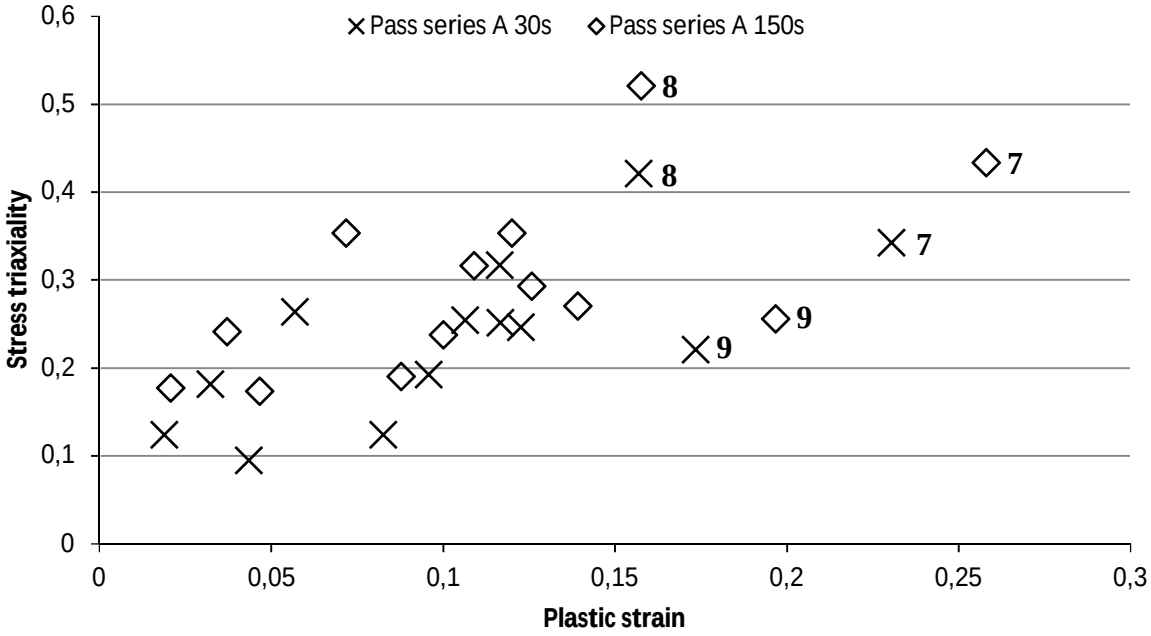

Figure 17. Stress triaxiality (σ_m/σ_{eq}) plotted against plastic strain in the centre of the ingot for all passes in series A with 30 and 150 seconds transportation time from the furnace.

5.4 Hydrostatic integration parameter

As discussed in chapter 2.6, the hydrostatic integration parameter (G_m) treats hydrostatic pressure and plastic strain as equally important when it comes to void closure. This makes it a bit unbalanced since previous work [19] has shown plastic strain to be more important. Despite this, G_m is a useful way of evaluating both single passes and entire pass series since it is a scalar. This makes it easy to compare the evolution of G_m and its relation to other parameters.

The hydrostatic integration parameter G_m, at the centre of the ingot, for each pass in series A and B, with 30 seconds transportation time from the furnace, is shown in figure 18. This plot shows the same trend as figure 16. There are five passes in series B that contribute markedly more than the others, while there are only two in series A. In both plots, the passes that stand out are the same. In figure 19, G_m values, as a result of variation of transport time from the furnace, are compared. Since both hydrostatic pressure and plastic strain increase, when a longer transportation time is used, the G_m value also increases.

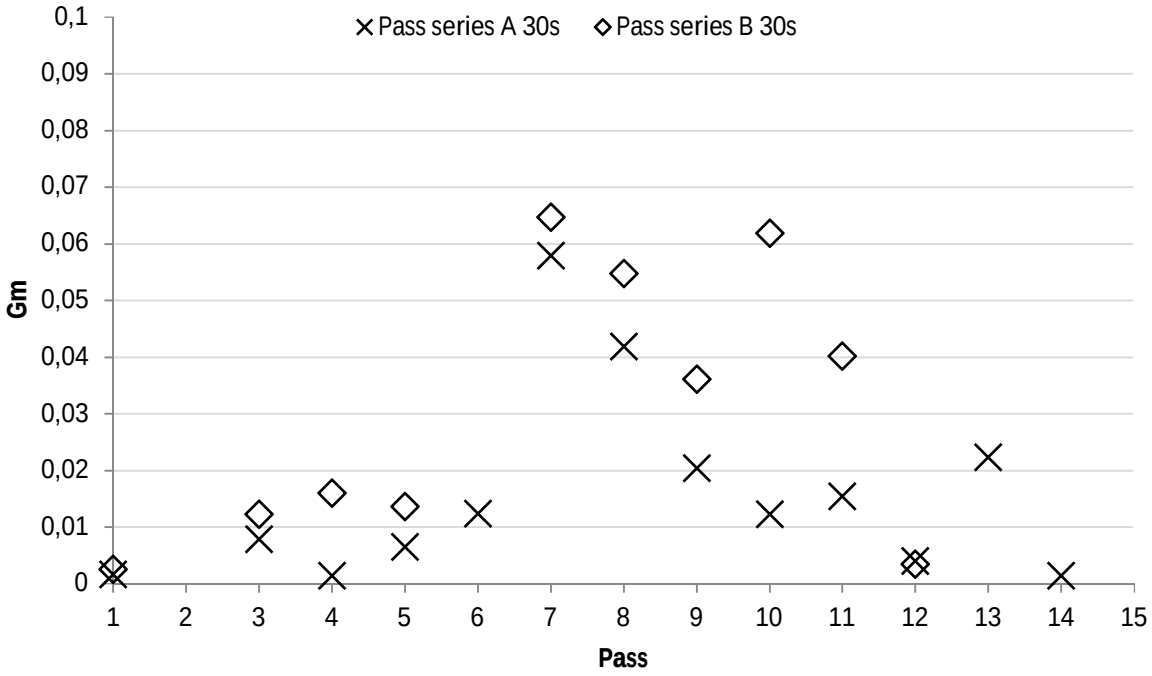

Figure 18. G_m at the centre of the ingot, for each pass in series A and B (30 seconds transportation time from the furnace).

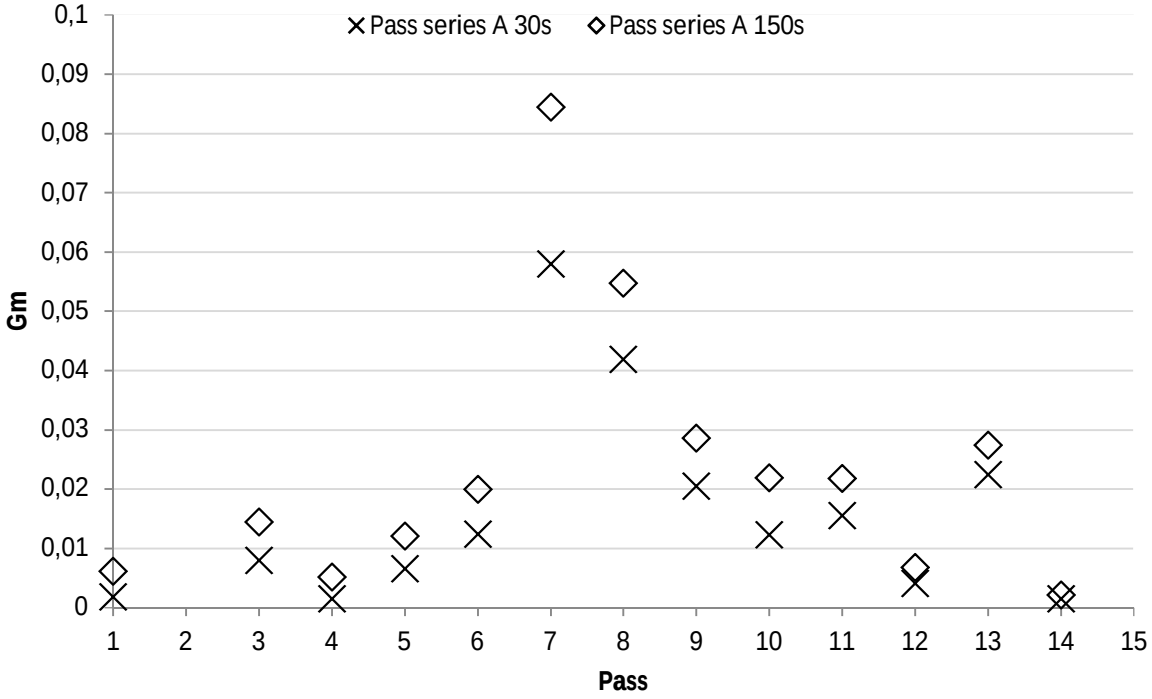

Figure 19. G_m at the centre of the ingot, for each pass in series A using both 30 and 150 seconds transportation time from the furnace.

A simplified way of evaluating the effect of different passes on the strain penetration and the ability to close voids would be to use the analytical parameter Δ. The correlation between Δ and G_m is visible in figure 20, where these parameters are plotted against each other for each simulated pass. It shows that G_m grows exponentially as Δ decreases, and at Δ values less than 1.80 the increase of G_m is extensive.

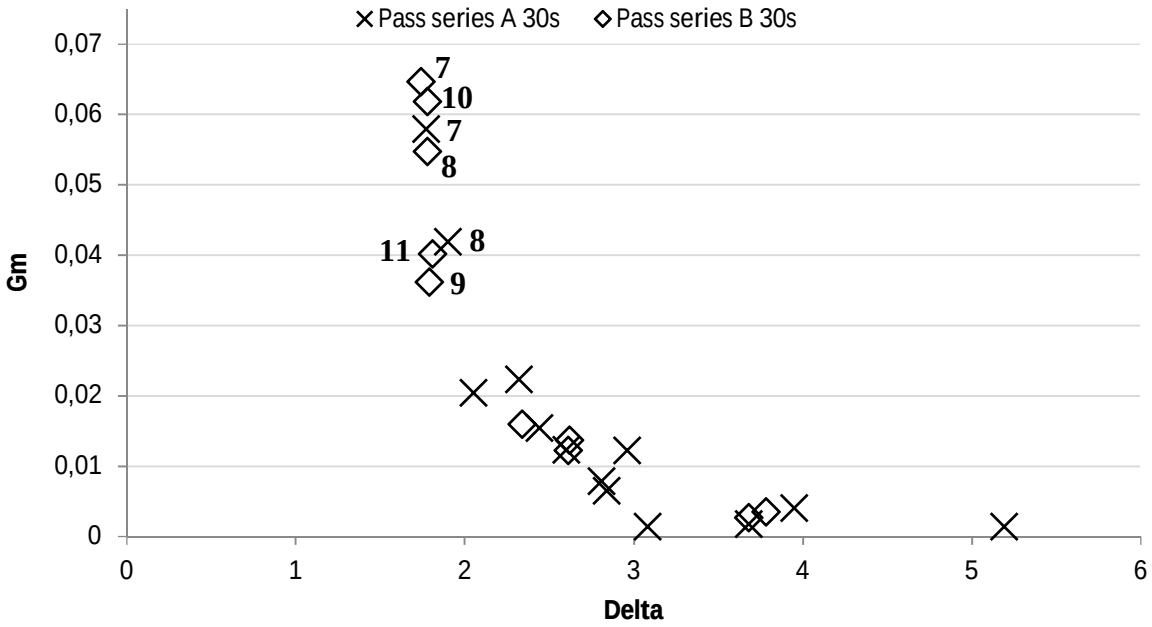

Figure 20. G_m plotted against Δ for all passes in series A and B using a 30 second transportation time from the furnace.

There are two main problems with the parameters that have been used to evaluate the pass series. First, it should be noted that they lack the ability to take into account turning of the ingot between passes. As discussed in chapter 2.5.3, a change of deformation direction increases the total plastic strain required to obtain a certain decrease of the void volume. Second, it is not possible to determine when voids of a specific volume and shape will be closed. Therefore, the results can only be used to compare different passes or pass series and cannot be used as exact threshold values.

The results show the effect of a change in the pass schedule on the ability to close voids. As an example, the model can be used to check if a change of a pass schedule changes the ability to close voids.

5.5 General recommendations

As a result of the simulations of pass series A and B, using both 30 and 150 seconds holding time, the effects on void closure ability are indicated for some general actions. The actions and their effects are shown in table 7 together with the criteria for them to be effective. It should however be noted that these recommendations are very general, and full simulations should be carried out to examine other pass series.

Table 7. General recommendations for improved void closure ability during hot rolling in the blooming mill, as a result of the simulation of pass series A and B with varying holding time.

	Action	Effect	Criterion	Source
Pass series	Increased reduction in specific passes.	Increased overall deformation. Increased contact length between roll and ingot, lower Δ.	$\Delta < 1.8$	Eq. 5 Fig. 18
Pass series	Increased total reduction between turnings of the ingot.	Beneficial if the void shape is decreased in one dimension.	Approximate $\sum \varepsilon_p > 0.4$ at the centre of the ingot	Ref [20] Fig. 7
Thermal gradient	Using a holding time between the furnace and blooming mill to achieve a cooler surface.	Increased deformation in the centre of the ingot due to lower σ_{eq} compared to the surface regions.		Ref [17] Fig.15
Roll diameter	Increased roll diameter, practically by selecting specific roll grooves.	Increased contact length between roll and ingot, lower Δ.		Eq. 5 Ref. [15]

6 Conclusions

By validating the parameterized model with measured roll separating forces and surface temperatures of the ingot, it has been shown to describe hot rolling in the blooming mill.

According to literature, increased hydrostatic stress and plastic strain, and therefore an increase of the hydrostatic integration parameter which is a combination of the two, imply better void closure ability for pass series B.

Strain penetration, hydrostatic stress, plastic strain and the hydrostatic integration parameter increase in pass series B, which reaches the same total reduction of the ingot in fewer passes compared to A.

Increased transportation time from the furnace has a positive effect on strain penetration, hydrostatic stress, plastic strain and the hydrostatic integration parameter.

The delta parameter (Δ) correlates well with the hydrostatic integration parameter (G_m), and can be used as a rule of thumb to ensure strain penetration and good void closure in the centre of the stock, when designing new pass series.

The FE model does however show that passes with similar values of Δ may get different properties in the centre of the ingot. This is particularly true for passes with Δ values below 1.8, which are the most important ones for void closure.

The model can be used as a supporting tool to develop new or adjust old pass series. Even though the focus during this thesis has been on the ability to close voids in the centre of ingots, other areas of interest can also be studied using the FE model.

7 Continued work

This thesis was carried out as a way of looking into the possibilities and usefulness of performing FE simulations of hot rolling in the blooming mill. The results have shown that the model can be used to evaluate the effect changes of pass schedules have on void closure ability. Even though the focus during this work has been on void closure, the FE model can be used in a variety of areas where it can deliver results that are hard to measure during the process. It should also be mentioned that the large span of different materials and dimensions that pass through the blooming mill leads to different aspects being important. Because of this, the cooperation between process and computational engineers is of great importance to maximize the benefits of using FE simulations to improve the industrial process.

Due to its somewhat general approach, there are a number of different subsections which would be of interest for future studies. Proposed future work can in this case be divided into two main groups, development of the FE model and experimental work.

Interesting areas for continued work when it comes to development of the model are:

- The implementation of a more complex material model is of great interest, since complex mechanisms like recrystallization etc. are known to occur in the process.

- Due to the long computational time, it is of interest to study different ways of reducing it. One way to potentially do this is to let a plate push the ingot throughout the entire simulation and use stationary rolls. This may reduce the number of iterations required in each time step and the number of time steps since the contact would be simplified. It would also make it easier for the model to converge.

- Studies including deformable rolls instead of rigid ones are of interest. This would include the effects of elastic deformation of the rolls and the increased contact length this leads to. Meshing the rolls would also make it possible to study the heat exchange between ingot and rolls.

Trials of different pass series in the blooming mill would be interesting experimental work to compliment and expand the use of the FE model. It would be of great interest if the parameters that are used in this work could be correlated to the evolution of void volume. This would require extensive work with sampling of specimens from the centre of rolled blooms and studies of remaining voids. Particularly interesting would be trials where specimens of the cross section from the stock could be taken both before and after the blooming mill. Trials like these are demanding, both when it comes to time and cost, but with this type of specimens the following projects would be possible:

- The effect on void closure and reopening, when turning the bloom 90 ° between two passes with large reductions, could be studied.

Since the material in the blooming mill has an as-cast structure in the beginning, and then undergoes different structural changes during rolling, it is of interest to study the microstructural evolution of different materials during the process. To utilize this in the FE model a new more complex material model has to be calibrated.

Bibliography

[1] M. software, "www.mscsoftware.com," [Online]. Available: http://www.mscsoftware.com/product/marc. [Accessed 29 06 2016].

[2] "Flat, Bar, and Shape Rolling," in *ASM Handbook 14 Forming and Forging*, ASM international, 1996, pp. 739-740.

[3] Sandvik, "www.smt.sandvik.com," [Online]. Available: http://smt.sandvik.com/se/materialcenter/materialdatablad/billets/sandvik-3r60/. [Accessed 29 06 2016].

[4] F. Humphreys and M. Hatherly, "Recovery after deformation," in *Recrystallization and related annealing phenomena*, Elsevier, 2004, pp. 169-210.

[5] F. Humphreys and M. Hartherly, "Recrystallization of single-phase alloys," in *Recrystallization and related annealing phenomena*, Elsevier, 2004, pp. 215-266.

[6] Y. Lin and X.-M. Chen, "A critical review of experimental results and constitutive descriptions for metals and alloys in hot working," *Material and design,* vol. 32, pp. 1733-1759, April 2011.

[7] S. Venugopal and P. Sivaprasad, "A journey with Prasad's processing maps," *Journal of materials engineering and performance,* no. 12, pp. 674-686, 2003.

[8] S. Venugopal, S. Mannan and Y. Prassad, "Processing map for mechanical working of stainless steel type AISI 316 L," *Scripta metallurgica et materiala,* vol. 28, pp. 715-720, 1993.

[9] L. Guiwu, H. Ying, Zhongqi Shi, S. Jiapeng, Z. Dening and Q. Guanjun, "Hot deformation and optimization of process parameters of an as-cast 6Mo superaustenitic stainless steel: A study with processing map," *Materials and design,* vol. 53, pp. 662-672, 2014.

[10] M. C. Mataya, E. R. Nilsson, E. L. Brown and G. Krauss, "Hot working and recrystallization of as-cast 316L," *Metallurgical and materials transactions A,* vol. 34A, pp. 1683-1703, 2003.

[11] S. K. Prasad and A. K. Gupta, "A constitutive description to predict high-temperature flow stress in austenitic stainless steel 316," *Procedia materials science,* vol. 6, pp. 347-353, 2014.

[12] A. He, X.-t. Wang, G.-l. Xie, X.-y. Yang and H.-l. Zhang, "Modified arrhenius-type constitutive model and artificial neural network-based model for constitutive relationship of 316LN stainless steel during hot deformation," *Journal of iron and steel research, international,* pp. 721-729, 2015.

[13] G. R. Johnson and W. H. Cook, "A constitutive model and data for metals subjected to large strains, high strain rates and high temperatures," in *Proceedings of the 7th international symposium on ballistics*, Den Haag, the Netherlands, 1983.

[14] I. Y. Tarnovskii, A. A. Pozdeyev and V. B. Lyashkov, Deformation of metals during rolling, London: Pergamon Press Ltd, 1965.

[15] W. A. Backofen, "Deformation processing," *Metallurgical transactions,* vol. 4, pp. 2679-2699, 1973.

[16] S. P. Dudra and Y.-T. Im, "Analysis of void closure in open-die forging," *Int. J. Mach. Tools Manufact.,* vol. 30, no. 1, pp. 65-75, 1988.

[17] M. Saby, P. Bouchard and M. Bernacki, "Void closure criteria for hot metal forming: A review," *Journal of manufacturing Process,* pp. 239-250, 2015.

[18] R. S. Nalawade, V. R. Marje, G. Balachandran and V. Balasubramania, "Effect of pass schedule and groove design on the metal deformation of 38MnVS6 in the initial passes of hot rolling," *Sadhana,* vol. 41, no. 1, pp. 111-124, 2016.

[19] M. Saby, P.-O. Bouchard and M. Bernacki, "A geometry-dependant model for void closure in hot metal forming," *Finite elements in analysis and design,* vol. 105, pp. 63-78, 2015.

[20] M. Saby, M. Bernacki, E. Roux and P.-O. Bouchard, "Three-dimensional analysis of real void closure at the meso-scale during hot metal forming processes," *Computational materials science,* vol. 77, pp. 194-201, 2013.

[21] R. D. Cook, D. S. Malkus, M. E. Plesha and R. J. Witt, Concepts and applications of finite element analysis, John Wiley & sons, inc., 2002.

[22] S. Yuan, L. Zhang, S. Liao, S. Jian, Y. Yu and M. Qi, "Simulation of deformation and temperature in multi-pass continous rolling by three-dimensional FEM," *Journal of materials processing technology,* no. 209, pp. 2760-2766, 2009.

[23] G. Sen-dong, Z. Li-wen, Y. Chong-xiang, R. Jin-hua, Z. Jian-lin and G. Hui-ju, "Multi-field coupled numerical simulation of microstructure evolution during the hot rolling process of GCr15 steel rod," *Computational materials science,* no. 50, pp. 1951-1957, 2011.

[24] Marc 2014.1 Volume A: Theory and user information, MSC Software corporation, 2014.

[25] L.-E. Lindgren, K. Domkin and S. Hansson, "Dislocations, vacancies and solute diffusion in physical based plasticity model for AISI 316L," *Mechanics of materials,* vol. 40, pp. 907-919, 2008.

[26] M. Fukuhara and A. Sanpei, "Elastic moduli and internal friction of low carbon and stainless steels as a function of temperature," *ISIJ international,* vol. 33, no. 4, pp. 508-512, 1993.

[27] K. C. Mills, Y. Su, Z. Li and R. F. Brooks, "Equations for the calculations of the thermo-physical properties of stainless steel," *ISIJ International,* vol. 44, no. 10, pp. 1661-1668, 2004.

[28] "Marc Python 2010: Tutorial and reference manual," MSC.Software Corporation, 2010.

[29] J. Beddoes and M. Bibby, "4.6 Rolling," in *Principles of metal manufacturing processes*, Elsevier, 2003, pp. 122-127.

[30] F. Qu, Z. Reng, R. Ma, Z. Wang and D. Chen, "The research on the constitutive modeling and hot working characteristics of as-cast V-5Cr-5Ti alloy during hot deformation," *Journal of alloys and compounds,* vol. 663, pp. 552-559, 2016.

[31] H. Bin, X. Ke, H. Kan and L. Hong, "Development of a geometric modelling strategy for roll pass optimal design," *Robotics and Computer-Integrated Manufacturing,* no. 30, pp. 622-628, 2014.

[32] M. Nakasaki, I. Takasu and H. Utsunomiya, "Application of hydrostatic integration parameter for free-forging and rolling," *Journal of materials processing technology,* pp. 521-524, 2006.

[33] M. Oyane, "Criteria of ductile fracture strain," vol. 15, no. 90, pp. 1507-1513, 1972.

Appendix A – python script used to wrap Marc/Mentat commands in the function py_send

The code in this appendix was used to wrap Marc/Mentat commands from a procedure file in the function py_send. The resulting .py-file was then used as a starting point to achieve the final parameterized script. The code comes from the manual “Marc Python 2010; Tutorial and reference manual” [28].

```
#
# create a python function from procedure file
# usage:
#   python py_create.py input.proc output.py
#      where
#        input.proc is the procedure filename
#        output.py  is the python script name
#
import sys
import string
def main(fnamei, fnameo):
    i = open(fnamei,"r")
    o = open(fnameo,"w")

    o.write("from py_mentat import *\n")
    o.write("def main():\n")
    for line in i.readlines():
      s = string.strip(line)
      if s == "":
        continue
#      print line
      st = "    py_send(\"%s\")\n" % s
      o.write(st)
    o.write("\n")
    o.write("if __name__ == '__main__':\n")
    o.write("    main()\n")

if __name__ == "__main__":
    main(sys.argv[1],sys.argv[2])
```